Stochastic DNA walker for electrochemical biosensing sensitized with gold nanocages@graphene nanoribbons

Qiumei Feng, Xiaolei Zhao, Yuehua Guo, Mingkai Liu, Po Wang

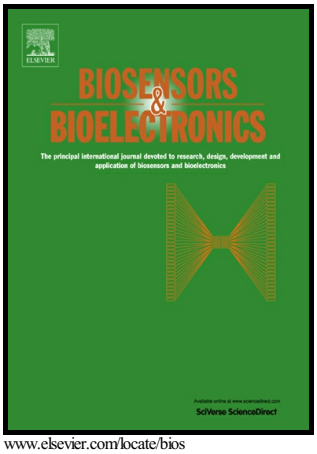

www.elsevier.com/locate/bios

PII: S0956-5663(18)30143-X
DOI: https://doi.org/10.1016/j.bios.2018.02.050
Reference: BIOS10312

To appear in: *Biosensors and Bioelectronic*

Received date: 17 November 2017
Revised date: 3 February 2018
Accepted date: 22 February 2018

Cite this article as: Qiumei Feng, Xiaolei Zhao, Yuehua Guo, Mingkai Liu and Po Wang, Stochastic DNA walker for electrochemical biosensing sensitized with gold nanocages@graphene nanoribbons, *Biosensors and Bioelectronic,* https://doi.org/10.1016/j.bios.2018.02.050

Stochastic DNA walker for electrochemical biosensing sensitized with gold nanocages@graphene nanoribbons

Qiumei Feng [a], Xiaolei Zhao [a], Yuehua Guo [b], Mingkai Liu [a,*], Po Wang [a,*]

[a] *School of Chemistry and Materials Science, Jiangsu Normal University, Xuzhou 221116, P. R. China*

[b] *Surgical Comprehensive Laboratory, Affiliated Hospital of Nantong University, Nantong 226001, P. R. China*

Abstract

A target-driven stochastic DNA walking electrochemical biosensor sensitized with gold nanocages@graphene nanoribbons (Au NCs@GNRs) was explored for sensitive detection of target DNA. Benefited from the large surface area and excellent conductivity of Au NCs and GNRs, the proposed sensing platform not only improved the electron transfer kinetics involved in electrochemical reactions, but also enhanced the loading capability for stem-loop structural DNA segment (H). Upon the addition of target DNA, the hairpin structure of H was opened and H:target DNA duplex was formed based on toehold-mediated DNA strand displacement. In the presence of exonuclease III (Exo III), the H:target DNA duplex was digested. As a result, target DNA spontaneously dissociated from H:target DNA duplex and then hybridized with another H strand. Therefore, the continuous locomotion of target DNA unceasingly triggered new digestion process from near to far along the electrode surface, resulting in great signal amplification. The proposed strategy exhibited excellent detection performances for DNA analysis in complex matrix such as human serum, which illuminated the practical application field of the sensing platform.

Keywords: Stochastic DNA walker; Gold nanocages; Graphene nanoribbons; Electrochemical detection; Signal amplification.

* Correspondence authors. Tel.: +86 516 83403165; fax: +86 516 83536977.

E-mail addresses: wangpo@jsnu.edu.cn; liumingkai@jsnu.edu.cn.

1. Introduction

Detection of specific DNA sequences at ultralow concentration is of great importance for environmental monitoring, clinical diagnostics, genetic diseases and biomedical applications (Dong et al., 2010; Huang et al., 2011). Relying on various transduction and amplification strategies, many approaches have been proposed, including polymerase chain reaction (PCR) (Marx and Strerath, 2005; Cheglakov et al., 2006), catalyzed hairpin assembly (Yin et al., 2008), rolling circle amplification (Zhao et al., 2008; Bi et al., 2010), entropy-driven catalysis (Lv et al., 2015) and DNA walking machine (Chen et al., 2015). Among them, DNA walking machine is one of the most promising methods because such machine can transfer cargoes from one location to another on the nanometer scale in the presence of the moving forces generated by fuels (Peng et al., 2017; Wang et al., 2017a; Xu et al., 2017; Zhang et al., 2018). Inspired by Sherman et al. (Sherman, 2009), various DNA walking machines were constructed on the surface of three-dimensional nanoparticles for fluorescent biosensing powered by nicking endonuclease (Ji et al., 2017; Yang et al., 2016; Zhang et al., 2015), exonuclease III (Exo III) (Qu et al., 2017), and DNA catalytic hairpin assembly reaction (Guo et al., 2017; Li et al., 2011). In these DNA walking systems, specific walking DNA strand was designed to move autonomously and multisteply along programmed nucleic acid tracks, resulting in great signal amplification (Wang et al., 2015a). Recently, it was reported that the mechanical translocation of nucleic acids on nucleic acid tracks was associated with solid heterogeneous sensing surface (Cai et al., 2016; Ji et al., 2017; Jung et al., 2017; Pu et al., 2017). On the electrode

surface, nicking endonuclease was employed to construct DNA walking machine for nucleic acid detection with hyperbranched rolling circle and large surface area of nanoparticles for signal amplification (Zhang et al., 2017). To further improve the measuring sensitivity for trace biological samples, seeking for a new DNA walking electrochemical sensor coupled with an efficient signal transduction device is promising.

To achieve a highly efficient electrochemical sensing platform, the combination of two (or more) types of nanostructure materials as the electrode material is not negligible (Wang et al., 2015b). For example, gold nanoparticles were decorated on graphene sheets to enhance the electrochemical signal response (Benyidi et al., 2015). Latterly, with the prominent optical, electric and catalytic properties, noble metals nanoparticles have attracted considerable attention in fundamental researches (Chen et al., 2015; Gai et al., 2015; Gu et al., 2017; Gao et al., 2017; Zhen et al., 2015). One interesting topic relating to this area was the exploitation of gold nanocages (Au NCs) since their large surface area and good conductivity were both hollow interiors and porous walls dependent (Wang et al., 2017c; Wang et al., 2014). Besides, retaining the feature of high length-diameter ratio and representing a particular kind of graphene-related material, graphene nanoribbons (GNRs) can be produced from unzipping carbon nanotubes (CNTs) (Kosynkin et al., 2009; Teeter et al., 2017). GNRs not only held superior mechanical properties, high thermal conductivity, plenty of space for chemical modification and electronic transport properties of graphene, but also possessed particular features such as straight edges, high length-to-width ratio

and excellent surface integration with less defects and/or holes on the basal plane (Higginbotham et al., 2010; Liu et al., 2014; Rafiee et al., 2010). Therefore, it is promising to design an efficient signal transduction platform by utilizing the combination of Au NCs and GNRs (Au NCs@GNRs).

Herein, taking advantage of the signal amplification of stochastic DNA walking strategy coupled with the excellent physicochemical properties of Au NCs@GNRs, an innovative electrochemical biosensor was constructed for quantitative analysis of target DNA. The fabrication procedure of the sensor and the moving mechanism of DNA walker were illustrated in Scheme 1. Firstly, Au NCs@GNRs suspension was dropped onto the surface of glassy carbon electrode (GCE) to improve electro-transfer capability and functional surface area. Then, a stem-loop structural hairpin DNA (H) was connected to Au NCs via Au-S bond. Upon the addition of target DNA, the hairpin structure was opened and H:target DNA duplex was formed based on toehold-mediated DNA strand displacement. Afterward, Exo III, which could selectively cleave double-stranded DNA from 3´-OH blunt or recessed end and had little role on single stranded DNA or 3´-overhang end of double-stranded DNA was introduced into the DNA walking system (Yang et al., 2015). Thus, the formed H:target DNA duplex on the modified electrode was digested and cleaved under the shearing of Exo III. After digesting, target DNA spontaneously dissociated from H:target DNA duplex and then hybridized with another H strand. So, the continuous locomotion of target DNA unceasingly triggered new digesting processes from near to far along the electrode surface. It should be noted that the overhang and stem

sequence near 5′ end of H strand could not be digested, which was applied as the capture DNA for probe. Finally, via toehold-mediated strand displacement reaction, ferrocene labelled probe (probe-Fc) was introduced to the electrode surface. Therefore, on the basis of the oxidation current response of Fc, a sensitive electrochemical biosensor for target DNA detection was successfully achieved.

Preferred position for Scheme 1

2. Experimental

2.1. Reagents and apparatus

Unless otherwise noted, all chemicals were obtained from Sigma-Aldrich (St. Louis, Mo, USA). CNTs with the diameter of 40-60 nm were purchased from Chengdu Organic Chemicals Co. Ltd. (Chengdu, China). Exo III was obtained from Takara Biotechnology Co. Ltd. (Dalian, China). Phosphate buffer solution (PBS, 0.1 M) was used for electrochemical detection. All other regents were of analytical grade and used without further purification. Ultrapure water from a Millipore water purification system (≥18 MΩ cm, Milli-Q, Millipore) was used throughout the experiment. All the oligonucleotides were purchased from Sangon Biotech. Co. Ltd. (Shanghai, China), and purified using high-performance liquid chromatography. Their sequences were listed as following:

H: 5′-SH-TGCAAAAGAGAATGGGTTTAGGGCGGGTTGGGAACCCATTCTCCC AGTTGATT-3′.

S1: 5′-SH-TTTTTTTTTT-3′.

Probe-Fc: 5′-AAACCCATTCTCTTTTGCA-Fc-3′.

S2: 5′-TGCAAAAGAGAAT-3′.

Target DNA: 5′-AATCAACTGGGAGAATGGGTTCCCAACCCTAACT-3′.

Non-terminal one-base mismatched DNA:

5′-AATCAACTCGGAGAATGGGTTCCCAACCCTAACT-3′.

5′ end one-base mismatched DNA:

5′-TATCAACTGGGAGAATGGGTTCCCAACCCTAACT-3′.

3′ end one-base mismatched DNA:

5′-AATCAACTGGGAGAATGGGTTCCCAACCCTAACG-3′.

Three-bases mismatched DNA:

5′-AATCAACTCGGAGAATCGGTTCCCTACCCTAACT-3′.

The underlined region of H identified the stem sequence, and mismatched bases for target DNA were highlighted in the boxes.

Electrochemical experiments including differential pulse voltammetry (DPV) and cyclic voltammetry (CV) were conducted on a CHI760D electrochemical workstation (CH Instruments, Austin, USA) at room temperature. A conventional three-electrode system was applied for all electrochemical experiments. The working electrode was a 3 mm diameter GCE, meanwhile, Pt wire and Ag/AgCl were served as the counter and reference electrodes, respectively. Electrochemical impedance spectroscopy (EIS) measurements were performed on a PGSTAT30/FRA2 system (Autolab, Netherland). Transmission electron microscopy (TEM) images were obtained on a JEM-2100 transmission electron microscope (JEOL Ltd., Japan). Scanning electron micrograph (SEM) was performed on an S-4800 microanalyzer (Hitachi, Japan).

2.2. Fabrication of GNRs suspension

GNRs were prepared by oxidative unzipping CNTs, which was performed according to literatures (Higginbotham et al., 2010; Liu et al., 2013). In detail, 500 mg of CNTs was poured into 100 mL of concentrated sulfuric acid (98%) under continuous stirring. After 1 h, 13 mL of phosphoric acid (H_3PO_4, 30%) was injected into the above solution. Then, 0.5 g $KMnO_4$ was added, and this process was repeated three times per 30 min. After finishing, the obtained mixture was cooled to room temperature and subsequently located into 1 L of ice water mixture containing H_2O_2 (15 mL, 30 wt%). The obtained mixture was kept at a standstill for 24 h to coagulate, and the precipitate was sonicated for 20 min with a power of 100 W. In order to remove excess oxidizing agents, the obtained samples were dialyzed for one week. Finally, the oxidized GNRs were reduced through the treating of hydriodic acid at 100 °C for 10 h to obtain GNRs.

2.3. Synthesis of Au NCs

Briefly, 400 μL of 3 mM Na_2S solution was added into the boiling 30 mL ethylene glycol in nitrogen atmosphere. After refluxing for 7 min, 7.5 mL of polyvinylpirrolidone (PVP, 200 mg mL^{-1}) was injected and incubated for 10 min. After that, 2.5 mL of 4.8 mg mL^{-1} silver nitrate solution was added into the above mixture and allowed to run until the color became metallic greenish brown, getting silver nanocubes. Then, to form Au NCs, 2.5 mL of $HAuCl_4$ (0.5 mM) was added into the mixed solution containing 25 mL PVP and 500 μL of the as-prepared silver

nanocubes colloid. Until the color was stable, the resulting products were cooled with ice water. To remove the formed AgCl and excess PVP, the products were centrifuged and washed with saturated NaCl solution for six times. The final deposit was resuspended in 1 mL water for further usage.

2.4. Electrode pretreatment and modification

Firstly, the homogeneous Au NCs@GNRs suspension was prepared by dispersing Au NCs into GNRs solution and then successively applied under ultrasonic wave for a period of 60 min. Subsequently, 10 μL of Au NCs@GNRs suspension was drop-cast onto the surface of glassy carbon electrode (GCE) and dried at room temperature. The acquired Au NCs@GNRs/GCE was immersed in 100 μL of the stem-loop structure H solution (0.5 μM) and incubated for 4 h at 4 °C. After rinsing, the resulting H modified electrode (H/Au NCs@GNRs/GCE) was submerged in 100 μL of PBS containing 0.5 μM S1 for 4 h to block the nonspecific binding sites of electrode surface. Prior to incubation, H and S1 were activated by Tris (2-carboxyethyl) phosphine hydrochloride (TCEP) to cut the S-S bond. Finally, S1/H/Au NCs@GNRs/GCE was rinsed extensively with PBS for subsequent usage.

2.5. Free-running process of DNA walker and electrochemical measurements

The free-running process of DNA walker was displayed in Scheme 1. Firstly, S1/H/Au NCs@GNRs/GCE was immersed in target DNA solution for 1 h at 37 °C. Then, after washing with PBS, the resulting target DNA/S1/H/Au NCs@GNRs/GCE was further immersed in Exo III solution (0.4 U μL^{-1}) for free-running process of DNA walker for 50 min. Afterward, the resulting electrode was incubated with

S2:probe-Fc duplex solution, which was the hybridization product of S2 (0.5 μM) and probe-Fc (0.5 μM) for 1 h at 37 °C. After rinsing, the sensing interface was detected in nitrogen atmosphere. DPV from 0 to 500 mV (vs. Ag/AgCl) with a pulse amplitude of 25 mV and quiet time of 2 s was performed to record the electrochemical response.

3. Results and discussion

3.1. Characterizations of nanomaterials

In this work, GNRs were fabricated by longitudinally unzipping of the pristine CNTs and the morphology of the resulting GNRs was characterized by TEM. As depicted in Fig. 1A and Fig. 1B, the edge of GNRs was rough and a wrinkled-layer structure with several stacking layers could be clearly observed. Moreover, no residual CNTs existed in the formed GNRs, indicating that the pristine CNTs were totally opened or unzipped. Besides, Fig. 1C displayed SEM image and TEM image of the synthesized Au NCs with particle size of about 50 nm and many pores at the walls. The as-prepared Au NCs possessed good uniformity, hollow interiors and many openings at the walls. Moreover, the lattice fringe spacing of the Au NCs was measured to be 0.235 nm based on HR-TEM image (data not shown), which matched the *d* value for Au (111) (Miao et al., 2018; Wang et al., 2017b).

In Fig. 1D, the electrochemical oxidation of Fc was comparatively studied at different electrode interfaces. In contrast to the electrochemical response of bare GCE (curve a), GNRs/GCE presented stronger oxidation peak current (curve b), indicating that GNRs effectively promoted the electron transfer kinetics involved in the electrochemical oxidation of Fc. Furthermore, the highest peak current was observed

for Au NCs@GNRs/GCE (curve c), which may attribute to the improvement of electroactive surface area and the outstanding electronic transmission ability of noble metal nanoparticles. The above results implied that Au NCs@GNRs composite was a suitable matrix for electrochemical oxidation of Fc.

Preferred position for Fig. 1

3.2. Electrochemical characterizations of the sensing system

To efficiently monitor the interfacial properties of the modified electrodes, EIS and CV were utilized to explore the assembly processes of the sensor step by step (Fig. 2A and Fig. 2B). The diameter of the high frequency semicircle reflected the interfacial charge transfer resistance (R_{ct}). Compared with bare GCE (curve a), Au NCs@GNRs/GCE (curve b) exhibited an almost straight line with a much lower resistance in EIS and the increasing of peak current in CV because the existence of Au NCs and GNRs led to the increase in the electron transfer kinetics of $[Fe(CN)_6]^{3-/4-}$. Then, the successive introduction of H (curve c), S1 (curve d) and target DNA (curve e) resulted in continual R_{ct} rising and CV signal decreasing. The above phenomenon was ascribed to the electrostatic repulsion between the electroactive $[Fe(CN)_6]^{3-/4-}$ and the abundant negative charges of DNA backbones. However, after the cleavage process by the treatment of Exo III (curve f), the R_{ct} value decreased remarkably and CV peak current increased, validating the continually cleavage process and the formation of shorter products of H on electrode surface. Finally, the probe on the resultant electrode interface caused significant rising of R_{ct} and decreasing of CV peak current (curve g), indicating the hybridization between the remaining part of H and

probe-Fc. The EIS measurements and CV responses demonstrated the successful preparation of the proposed sensor.

Preferred position for Fig. 2

3.3. Optimization of experimental conditions

According to literature, the electrical conductivity of carbon-based electrode was greatly influenced by the amount of carbonaceous materials (Tran et al., 2013). Thus, the effect of GNRs concentration on the current response of Fc was discussed (Fig. 3A). With the increase of GNRs concentration, the peak current increased gradually and achieved the maximum at 0.21 mg mL^{-1}. However, further increase of GNRs concentration resulted in a slight decrease in current signal. In addition, the electrochemical behavior of Fc was significantly influenced by the pH value of supporting electrolyte at the Au NCs@GNRs/GCE (Fig. 3B). The oxidation peak potential of Fc shifted slightly with the change of supporting electrolyte pH from 3.0 to 10.0. The largest peak current of Fc at Au NCs@GNRs/GCE was obtained in pH 6.0 PBS. Therefore, 0.21 mg mL^{-1} GNRs and pH 6.0 PBS were chosen for the following electrochemical experiments.

To achieve the goal of target DNA determination, the amount of Exo III and enzymatic cleavage time were also examined. Obviously, with the increasing concentration of Exo III, the oxidation peak currents increased and achieved a plateau at 0.4 U μL^{-1} (Fig. 3C). Thus, 0.4 U μL^{-1} Exo III was chosen for the latter assay. Besides, after the incubation of Exo III, the current signal reached the maximum at the

reaction time of 50 min (Fig. 3D), demonstrating that 50 min incubation was enough for the cleavage process.

Preferred position for Fig. 3

3.4. Analytical applications

To explore the quantitative detection performance of the designed DNA walking biosensor, various concentrations of target DNA were assayed under the optimized experimental conditions. As can be seen from Fig. 4A, with the increase in target DNA concentrations, the oxidation peak currents of Fc increased correspondingly. The peak currents of Fc were linearly proportional to the logarithmic values of target DNA concentrations ranging from 1 fM to 100 pM, with a correlation coefficient of 0.9919 (Fig. 4B). The low detection limit of 600 aM was obtained for target DNA based on the signal to noise ratio of 3, which was much lower than some existing DNA assays (Mei and Tang, 2017; Ensafi et al., 2017). In addition, the relative standard deviation (R.S.D.) for eight electrodes under the same conditions was 5.8% for 100 pM target DNA detection, indicating an acceptable fabrication reproducibility of the sensor. Besides, to evaluate the practical application ability of the stochastic DNA walking electrochemical sensor, target DNA was spiked into 10% human serum which could simulate the situation of real sample. The recoveries were 95% (for 100 fM) and 106% (for 100 pM), respectively, demonstrating the potential of the system in real sample analysis.

Preferred position for Fig. 4

3.5. Selectivity of the biosensor

The selectivity of the stochastic DNA walking sensor for DNA analysis was investigated by measuring the peak current responses to different DNA sequences, including complementary target DNA, one-base mismatched DNA, and three-base mismatched DNA. As recorded in Fig. 5, in contrast to the current signal of blank solution without DNA (bar a), no significant signal change was observed for three-base mismatched DNA (bar b), while a relatively small current response was obtained for non-terminal one-base mismatched DNA (bar c). However, when the detection system was incubated with complementary target DNA, the peak current increased remarkably (bar d). Such results indicated that the developed sensor possessed excellent sequence specificity. Moreover, the one-base mismatched DNA at both 5′ end and 3′ end were also investigated. When the one-base mismatch occurred at the 5′ end of target DNA (bar e), the current signal was slightly lower than that of non-terminal one-base mismatched DNA (bar c). In this case, the H:target DNA duplex cannot be digested by Exo III because of the mismatched behavior, resulting in very weak signal response. However, when the one-base mismatch occurred at the 3′ end of target DNA (bar f), there was no obvious current change in comparison with that of target DNA. To avoid the Exo III digestion of target DNA in H:target DNA duplex, some extra bases (TAACT) at the 3′ end of target DNA were not complementary to H, which were not involved in hybridization reaction. Therefore, the influence of one-base mismatch at 3′ end on current signal was negligible.

Preferred position for Fig. 5

4. Conclusions

In summary, based on a target-driven stochastic DNA walking system in combination with the excellent interfacial properties Au NCs@GNRs composite, an innovative signal amplification electrochemical biosensor was constructed for ultrasensitive detection of target DNA. The proposed strategy had brought forth the following novel points. Firstly, the stochastic DNA walking system could transport target DNA from one location to another on the electrode surface driven by Exo III, giving rise to considerably detectable signal amplification. Secondly, Au NCs with porous structure and large surface area could greatly improve the electron communication ability and provide more active sites for the immobilization of DNA strands. Moreover, the introduction of GNRs not only enhanced the charge transfer, but also resulted in a higher specific capacitance of Au NCs, by acting as "bridges" between Au NCs and electrode. Considering these advantages, the well-designed electrochemical biosensor showed good accuracy and precision for DNA detection in complex matrixes such as human serum, indicating a promising application in practical samples.

Acknowledgments

We gratefully acknowledge the National Natural Science Foundation of China (No. 21705062, 21675067), the Natural Science Foundation of Jiangsu Province (BK20170228), the Natural Science Foundation of Jiangsu Normal University (16XLR012), the State Key Laboratory of Analytical Chemistry for Life Science (SKLACLS1806), and the project funded by the Priority Academic Program Development of Jiangsu Higher Education Institutions.

References

Benyidi, A., Firouzabadi, A.D., Moshtaghiun, S.M., Mazloum, M., Tezerjani, M.D., 2015. Anal. Biochem. 484, 24–30.

Bi, S., Li, L., Zhang, S.S., 2010. Anal. Chem. 82, 9447–9454.

Cai, S.X., Chen, M., Liu, M.M., He, W.H., Liu, Z.J., Wu, D.Z., Xia, Y.K., Yang, H.H., Chen. J.H., 2016. Biosens. Bioelectron. 85, 184–189.

Cheglakov, Z., Weizmann, Y., Beissenhirtz, M.K., Willner, I., 2006. Chem. Commun. 30, 3205–3207.

Chen, Y., Xiang, Y., Yuan, R., Chai, Y.Q., 2015. Nanoscale 7, 981–986.

Chen, Z., Li, J., Chen, X., Cao, J., Zhang, J., Min, Q., Zhu, J.J., 2015. J. Am. Chem. Soc. 137, 1903–1908.

Dong, H.F., Gao, W.C., Yan, F., Ji, H.X., Ju, H.X., 2010. Anal. Chem. 82, 5511–5517.

Ensafi, A.A., Nasr-Esfahani, P., Rezaei, B., 2017. Sensor. Actuat. B-Chem. 249, 149–155.

Gai, P., Song, R., Zhu, C., Ji, Y., Chen, Y., Zhang, J.R., Zhu, J.J., 2015. Chem. Commun. 51, 14735–14738.

Gao, F., Zhou, F., Yao, Y., Zhang, Y., Du, L., Geng, D., Wang, P., 2017. J. Electroanal. Chem. 803, 165–172.

Gu, Y., Song, J., Li, M.X., Zhang, T.T., Zhao, W., Xu, J.J., Liu, M., Chen, H.Y., 2017. Anal. Chem. 89, 10585–10591.

Guo, Y.H., Wu, J., Ju, H.X., 2015. Chem. Sci. 6, 4318–4323.

Higginbotham, A.L., Kosynkin, D.V., Sinitskii, A., Sun, Z., Tour, J.M., 2010. ACS Nano 4, 2059–2069.

Huang, J., Wu, Y.R., Chen, Y., Zhu, Z., Yang, X.H., Yang, C.Y., Wang, K.M., Tan, W.H.,

2011. Angew. Chem., Int. Ed. 50, 401–404.

Ji, Y.H., Zhang, L., Zhu, L.Y., Lei, J.P., Wu, J., Ju, H.X., 2017. Biosens. Bioelectron. 96, 201–205.

Jung, C., Allen, P.B., Ellington, A.D., 2017. ACS Nano 11, 8047–8054.

Kosynkin, D.V., Higginbotham, A.L., Sinitskii, A., Lomeda, J.R., Dimiev, A., Price, B.K., Tour, J.M., 2009. Nature 458, 872–875.

Li, B., Ellington, A.D., Chen, X., 2011. Nucleic Acids Res. 39, 1–13.

Li, M.X., Zhao, W., Qian, G.S., Feng, Q.M., Xu, J.J. Chen, H.Y., 2016, Chem. Commun. 52, 14230–14233.

Liu, M.K., Song, Y.F., He, S.X., Tjiu, W.W., Pan, J.S., Xia, Y.Y., Liu, T.X., 2014. ACS Appl. Mater. Inter. 6, 4214–4222.

Lv, Y.F., Cui, L., Peng, R.Z., Zhao, Z.L., Qiu, L.P., Chen, H.P., Jin, C., Zhang, X.B., Tan, W.H., 2015. Anal. Chem. 87, 11714–11720.

Marx, A., Strerath, M., 2005. Angew. Chem. Int. Ed. 44, 7842–7849.

Mei, Z., Tang, L., 2017. Anal. Chem. 89, 633–639.

Miao, X., Cheng, Z., Ma, H., Li, Z., Xue, N., Wang, P., 2018. Anal. Chem. 90, 1098–1103.

Peng, L., Zhang, P., Chai, Y., Yuan, R., 2017. Anal. Chem. 89, 5036–5042.

Pu, Q.L., Li, J.L., Qiu, J.H., Yang, X.H., Li, Y., Yin, D., Zhang, X.Y., Tao, Y.Y., Sheng, S.C., Xie, G.M., 2017. Biosens. Bioelectron. 94, 719–727.

Qu, X.M., Zhu, D., Yao, G.B., Su, S., Chao, J., Liu, H.J., Zuo, X.L., Wang, L.H., Shi, J.Y., Wang, L.H., Huang, W., Pei, H., Fan, C.H., 2017. Angew. Chem. Int. Ed. 56, 1855–1858.

Rafiee, M.A., Lu, W., Thomas, A.V., Zandiatashbar, A., Rafiee, J., Tour, J.M. Koratkar, N.A., 2010. ACS Nano 4, 7415–7420.

Sherman, W., 2009. Science 324, 46–47.

Teeter, J.D., Costa, P.S., Pour, M.M., Miller, D.P., Zurek, E., Enders, A., Sinitskii, A., 2017. Chem. Commun. 53, 8463–8466.

Tran, H.V., Piro, B., Reisberg, S., Duc, H.T., Pham, M.C., 2013. Anal. Chem. 85, 8469–8474.

Wang, D., Vietz, C., Schröder, T., Acuna, G., Lalkens, B., Tinnefeld, P., 2017a. Nano Lett. 17, 5368–5374.

Wang, L.D., Deng, R.J., Li, J.H., 2015a. Chem. Sci. 6, 6777–6782.

Wang, P., Han, P., Dong, L., Miao, X., 2015b. Electrochem. Commun. 61, 36–39.

Wang, P., Wang, M., Zhou, F., Yang, G., Qu, L., Miao, X., 2017b. Electrochem. Commun. 81, 74–78.

Wang, X.Q., Gao, F., Zhang, X. Z., 2017c. Angew. Chem. Int. Ed. 56, 9029–9033.

Wang, Z.Z., Chen, Z.W., Liu, Z., Shi, P., Dong, K., Ju, E.G., Ren, J.S., Qu, X.G., 2014. Biomaterials 35, 9678–9688.

Xu, Z., Liao, L., Chai, Y., Wang, H., Yuan, R., 2017. Anal. Chem. 89, 8282–8287.

Yang, K.L., Huo, M., Guo, Y.H., Yang, Y.Z., Wu, J., Ding, L., Ju, H.X., 2017. Analyst, 142, 3740–3746.

Yang, X.L., Tang, Y.N., Mason, S.D., Chen, J.B., Li, F., 2016. ACS Nano 10, 2324–2330.

Yin, P., Choi, H.M., Calvert, C.R., Pierce, N.A., 2008. Nature 451, 318–322.

Zhang, H.Y., Lai, M.D., Zuehlke, A., Peng, H.Y., Li, X.F., Le, X.C., 2015. Angew. Chem. Int. Ed. 54, 14326–14330.

Zhang, J., Wang, L.L., Hou, M.F., Xia, Y.K., He, W.H., Yan, A., Weng, Y.P., Zeng, L.P., Chen, J.H., 2018. Biosens. Bioelectron. 102, 33–40.

Zhang, Y., Wang, L.X., Luo, F., Qiu, B., Guo, L.H., Weng, Z.Q., Lin, Z.Y., Chen, G.N., 2017. Chem. Commun. 53, 2910–2913.

Zhao, W., Ali, M.M., Brook, M.A., Li, Y., 2008. Angew. Chem., Int. Ed. 47, 6330–6337.

Figure captions

Scheme 1. Schematic illustration of stochastic DNA walking electrochemical biosensor sensitized with Au NCs@GNRs. Herein, the stem-loop structural DNA (H) was connected to Au NCs via Au–S bond, S1 was applied to block the nonspecific binding sites of Au NCs, which was propitious to target DNA walking. With the addition of target DNA, the hairpin structure of H was opened based on DNA strand displacement, resulting in H:target DNA duplex. Afterward, Exo III was introduced into the DNA walking system, and the H:target DNA duplex was digested under the shearing of Exo III. Then, target DNA spontaneously dissociated from H:target DNA duplex and hybridized with another H strand, and the continuous locomotion of target DNA unceasingly triggered new digestion process from near to far. Finally, via toehold-mediated strand displacement reaction, probe-Fc was introduced to the electrode surface, generating current signal for DNA sensing. It should be noted that S2 was used to hybridize with probe-Fc before strand displacement, the role of S2 was to protect hairpin H from hybridization with probe-Fc before target-triggered Exo III digestion.

Fig. 1. TEM images of GNRs (A) at low magnification and (B) at high magnification. (C) SEM image and TEM image (inset) of Au NCs. (D) Background-subtracted DPV responses of 20 μM Fc at bare GCE (a), GNRs/GCE (b), and Au NCs@GNRs/GCE (c). The TEM images of GNRs exhibited wrinkled-layer structure with several stacking layers, and the morphologic characterization of Au NCs displayed relatively uniform size of about 50 nm with hollow interiors and porous walls. The DPV signals demonstrated that both Au NCs and GNRs effectively promoted the electron transfer kinetics involved in the oxidation of Fc, suggesting that Au NCs@GNRs composite

was a suitable matrix for Fc oxidation.

Fig. 2. EIS plots (A) and CV curves (B) of different modified electrodes in 5 mM $[Fe(CN)_6]^{3-/4-}$ containing 0.1 M KCl: (a) bare GCE; (b) Au NCs@GNRs/GCE; (c) H/Au NCs@GNRs/GCE; (d) S1/H/Au NCs@GNRs/GCE; (e) S1/H/Au NCs@GNRs/GCE incubated with 10 pM target DNA; (f) target DNA/S1/H/Au NCs@GNRs/GCE treated by Exo III; (g) f incubated with S2:probe-Fc duplex solution. EIS parameters: DC potential, 0.27 V; frequency range, 10^5–0.01 Hz; amplitude, 0.005 V. For EIS characterization, Au NCs@GNRs/GCE (curve b) exhibited a much lower resistance in contrast to bare GCE (curve a), while the successive introduction of H (curve c), S1 (curve d), and target DNA (curve e) resulted in continual R_{ct} rising. However, the R_{ct} value decreased remarkably after Exo III digestion (curve f), and the hybridization between the remaining part of H and probe-Fc caused the resistance increase (curve g). For the CV responses of these electrochemical interfaces, the signal changes were not as obvious as those of EIS. However, in comparison with the current intensity of bare GCE (curve a), 113%, 89.6%, 76.1%, 68.5%, 81.1%, and 71.7% signal responses were obtained for curves b–g, respectively. The CV characterizations of these sensing interfaces were in agreement with EIS measurements, validating the assembly processes of the sensor step by step.

Fig. 3. (A) Effect of GNRs concentration on the oxidation peak current of 20 μM Fc at Au NCs@GNRs/GCE. (B) Background-subtracted DPVs of 20 μM Fc at Au NCs@GNRs/GCE in 0.1 M PBS with various pH values (from a to h: 3.0 to 10.0). (C) Effect of Exo III amount on the DPV response of the sensor. (D) Effect of Exo III nicking time on the DPV response of the sensor. The results revealed that 0.21 mg mL^{-1} GNRs was the optimum condition for electrode preparation, pH 6.0 PBS was

favorable for the enhancement of current sensitivity of Fc, 0.4 U μL^{-1} Exo III was sufficient for the digestion of DNA, and the optimum incubation time was 50 min for enzyme reaction.

Fig. 4. (A) Background-subtracted DPVs of the designed DNA walking biosensor for different concentrations of target DNA (from a to f: 1 fM, 10 fM, 100 fM, 1 pM, 10 pM and 100 pM). (B) The linear relationship between peak currents and the logarithms of DNA concentrations. The quantitative analysis of DNA demonstrated that the peak currents of Fc were linearly proportional to the logarithmic values of target DNA concentrations ranging from 1 fM to 100 pM, with a low detection limit of 600 aM at the signal to noise ratio of 3.

Fig. 5. Bar graph of the peak currents for different DNA sequences (100 pM): (a) blank solution, (b) three-base mismatched DNA, (c) non-terminal one-base mismatched DNA, (d) target DNA, (e) 5′ end one-base mismatched DNA, and (f) 3′ end one-base mismatched DNA. In contrast to the current signal of blank solution without DNA (bar a), no significant signal change was observed for three-base mismatched DNA (bar b), a relatively small current response was obtained for non-terminal one-base mismatched DNA (bar c), while the peak current increased remarkably for complementary target DNA (bar d), indicating excellent sequence specificity of the sensor. Moreover, when the one-base mismatch occurred at the 5′ end of target DNA (bar e), the current signal was slightly lower than that of non-terminal one-base mismatched DNA. When the one-base mismatch occurred at the 3′ end of target DNA (bar f), there was no obvious current change in comparison with that of target DNA, which was ascribed to the unique detection mechanism of the sensing platform.

Scheme 1

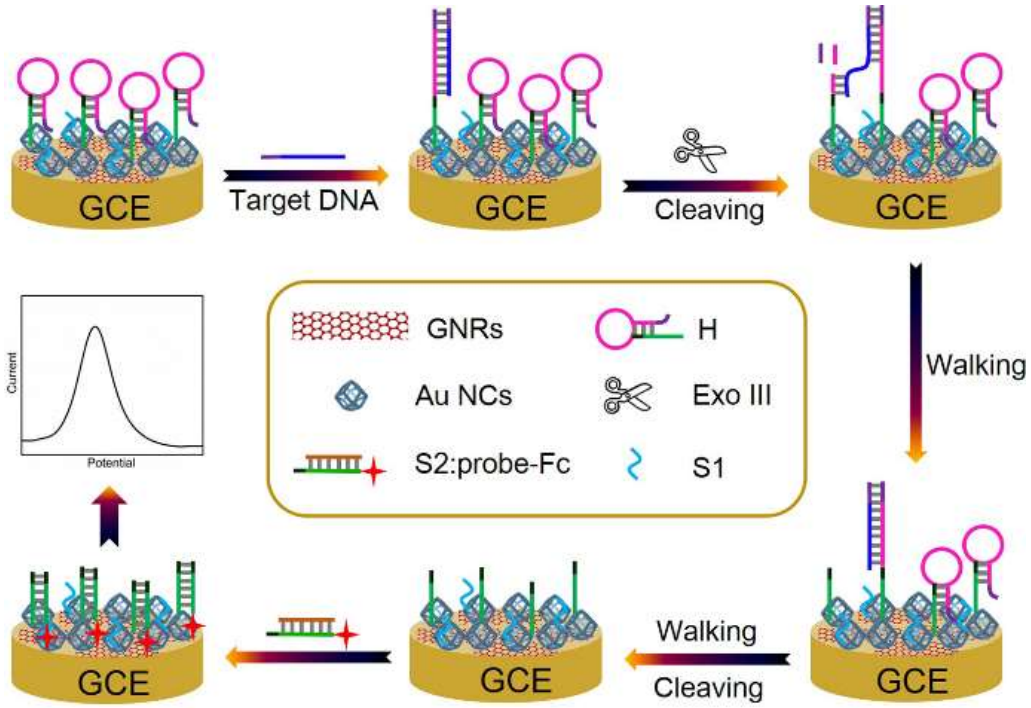

Fig. 1

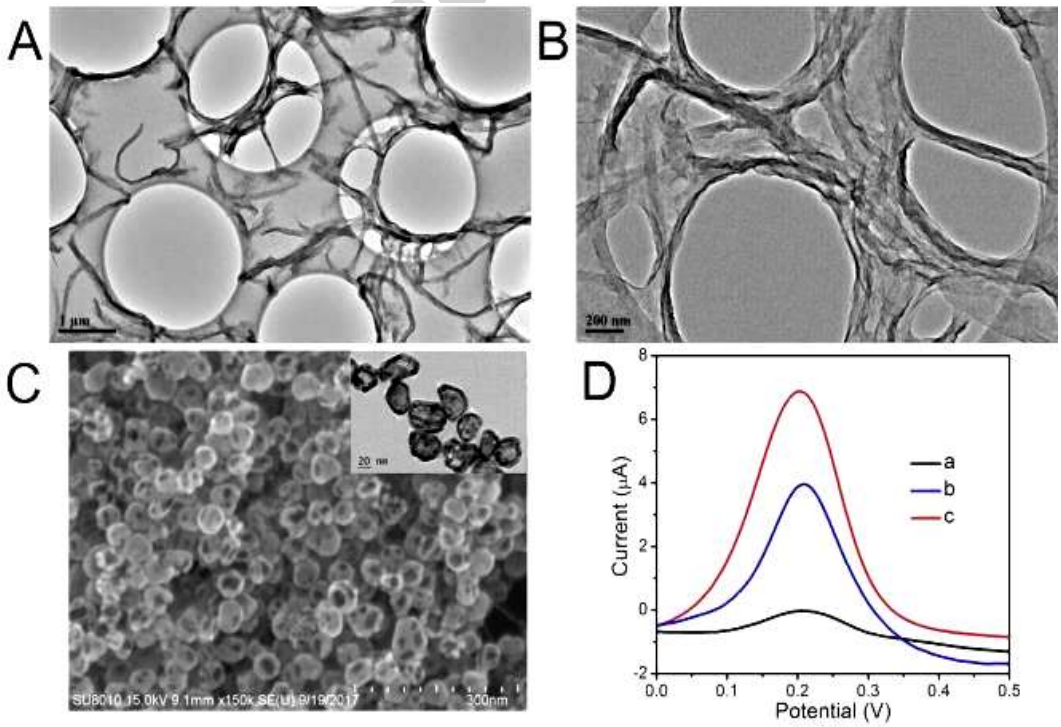

Fig. 2

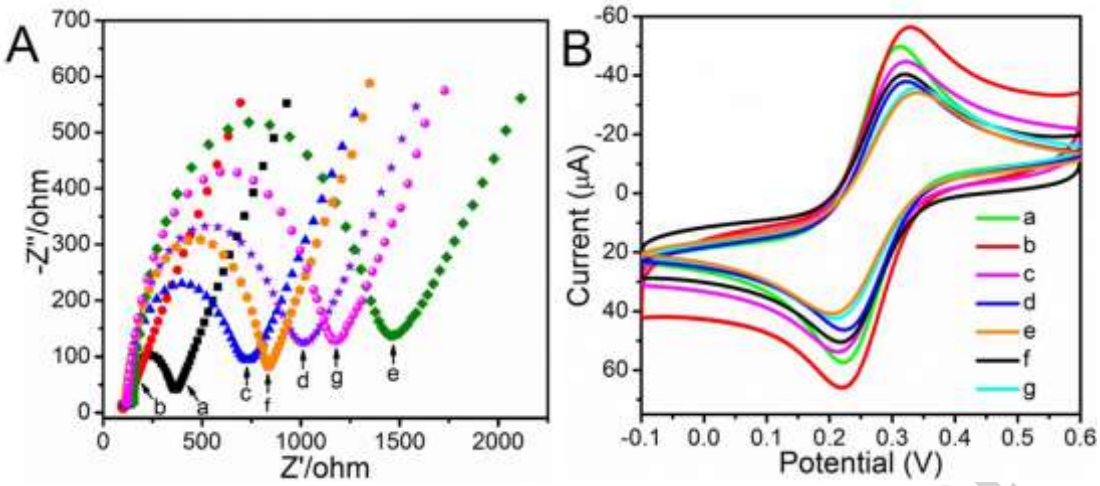
A
-Z''/ohm
Z'/ohm
a
b
c
d
e
f
g
B
Current (μA)
Potential (V)

Fig. 3

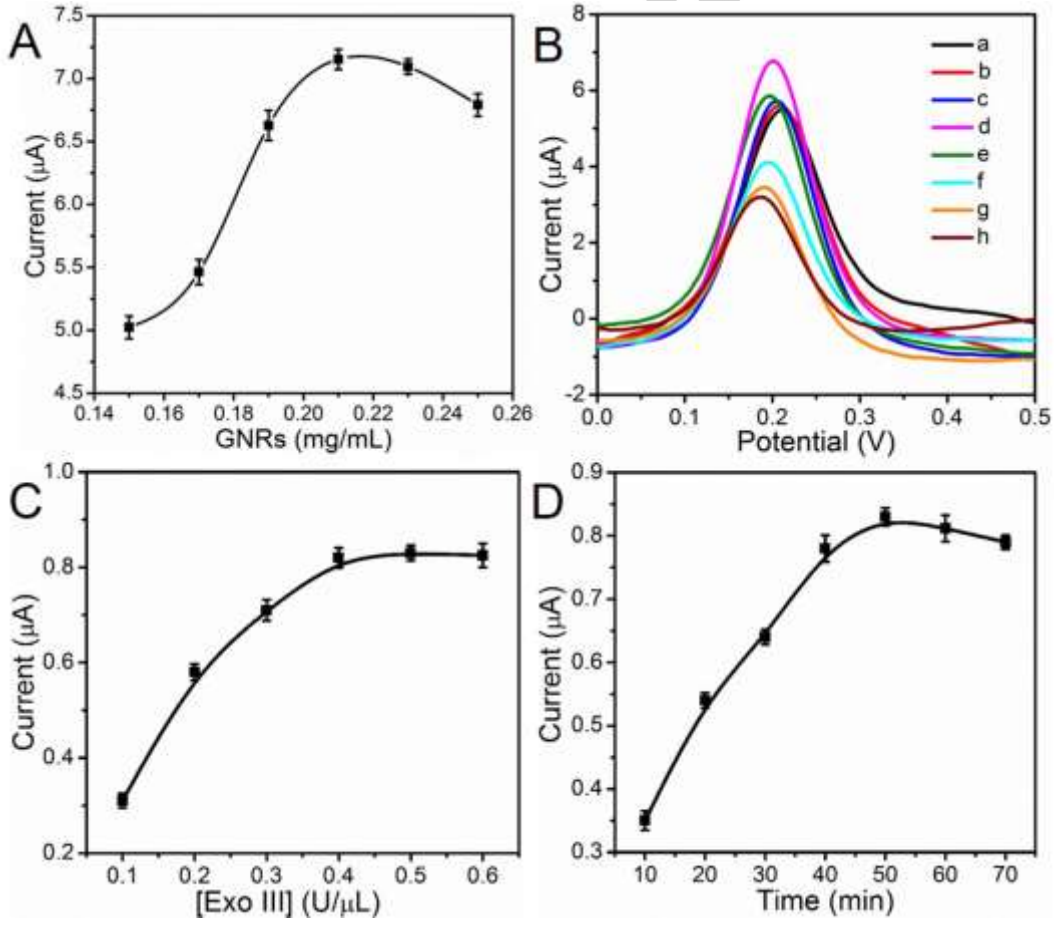
A
Current (μA)
GNRs (mg/mL)
B
Current (μA)
Potential (V)
a
b
c
d
e
f
g
h
C
Current (μA)
[Exo III] (U/μL)
D
Current (μA)
Time (min)

Fig. 4

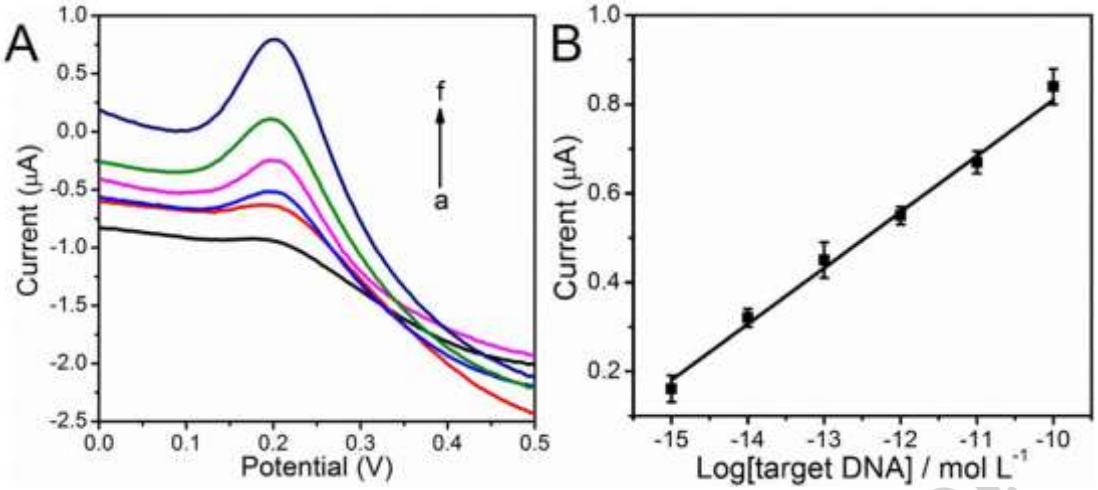
A
B
Current (μA)
Potential (V)
f
a
Log[target DNA] / mol L-1

Fig. 5

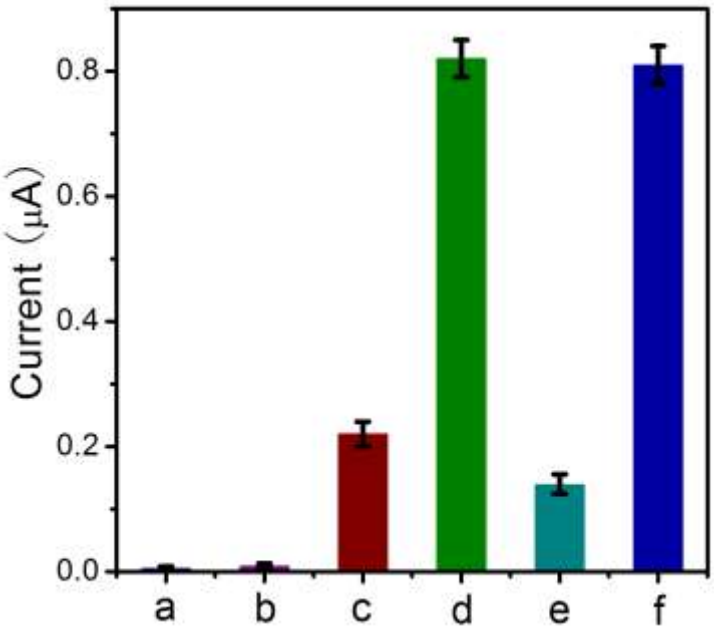
Current (μA)
a
b
c
d
e
f

Highlights

► A stochastic DNA walking electrochemical biosensor sensitized with gold nanocages@graphene nanoribbons was designed.

► In DNA walking system, target DNA transported from one location to another on electrode surface, realizing significant signal amplification.

► Gold nanocages improved the electron communication ability and provided sufficient active sites for the immobilization of DNA strands.

► Graphene nanoribbons enhanced the capacitance of gold nanocages, by acting as "bridges" between gold nanocages and electrode.